In: *Nonlinear Signal Processing in Medicine*, Ed. M. Akay, IEEE Press, 1999

Measurement and Quantification of Spatio-Temporal Dynamics of Human Epileptic Seizures

L. D. Iasemidis[*#^], J. C. Principe[*], J. C. Sackellares[#+~]

Departments of Electrical Engineering [*], Neurology [+] and Neuroscience [#]
University of Florida, Gainesville, FL 32610
Research [^] and Neurology [~] Service
VA Medical Center, Gainesville, FL 32608

I- Introduction

Since its discovery by Hans Berger in 1929, the electroencephalogram (EEG) has been the most utilized signal to clinically assess brain function. The enormous complexity of the EEG signal, both in time and space, should not surprise us since the EEG is a direct correlate of brain function. If the system to be probed is complex and our signal is a reliable descriptor of its function, then we can also expect complexity in the signal. Unfortunately, traditional signal processing (SP) theory is based on very simple assumptions about the system that produced the signal (e.g. linearity assumption). Hence the application of SP methodologies to automatically quantify the EEG has met the challenge with varying degrees of success. We can say that today the trained electroencephalographer or neurologist are still the golden standards in characterizing phasic events in the EEG such as spikes, the quantification of background activity (as in sleep staging) and identification and localization of epileptic seizures.

The status quo is not going to change overnight, but this paper will report on an exciting and promising new methodology to quantify the EEG that is rooted in the theory of nonlinear dynamics. EEG characteristics such as alpha activity and seizures (limit cycles [1]), instances of bursting behavior during light sleep, amplitude dependent frequency behavior (the smaller the amplitude the higher the EEG frequency) and existence of frequency harmonics (e.g. under photic driving conditions) are extensively reported in the clinical literature. All these characteristics also belong to the long catalog of typical properties of nonlinear systems. By applying techniques from nonlinear dynamics, several researchers have provided evidence that the EEG is a nonlinear signal with deterministic and perhaps chaotic properties (for a review see [1-9]).

This paper will address the quantification of EEG in epilepsy. Epilepsy is a group of disorders characterized by recurrent paroxysmal electrical discharges of the cerebral cortex that result in intermittent disturbances of brain function [10]. The bulk of research into human epilepsy has emphasized the description and categorization of the clinical and electroencephalographic features of seizures, defining clinical features of various epileptic syndromes and correlating clinical and electroencephalographic features with anatomical lesions of the brain or with genetic disorders. However, all this work has not addressed the essential feature of epilepsy, which is the fact that seizures occur intermittently, that is, seizure generation (and eventually epilepsy) is a dysfunction of brain dynamics.

Our group, employing analytical techniques developed for the analysis of complex nonlinear systems, was the first to demonstrate and quantify specific spatio-temporal dynamical changes in the EEG that begin *several minutes* before and end several minutes after a seizure [11-13]. These changes appear to evolve in a characteristic pattern, culminating in a seizure. Our current work indicates that, in the near future, we will obtain for the first time a signal processing methodology capable of quantifying the EEG more accurately and in a finer detail than it is possible to do through clinical evaluation. This should not come as a surprise because we are employing an analysis of dynamical patterns on a spatio-temporal trajectory, i.e. information that is not directly accessible from observing the EEG with the naked eye. As the theory of nonlinear dynamics clearly shows [14], state space is the natural domain to quantify properties of nonlinear dynamical systems. These properties may be undetectable in the time domain of the system output, i.e. the EEG tracing.

The measures we have employed do not assume any particular nonlinear model, nor do they depend upon *a priori* detailed understanding of the underlying mechanisms responsible for the generation of the data to be analyzed. They belong therefore to the class of non-parametric approaches. We have to further state that the general theory of nonlinear dynamical systems [14] does not rigorously describe brain dynamics. The brain is not an autonomous system. Its interaction with the environment creates a never-ending sequence of dynamical states where the brain internal dynamics are the overwhelming defining factor. Therefore, we have to realize that there is *a physiological time scale for brain dynamics*. Dynamical measures should therefore be computed within this time scale. Failing to realize this fact leads to the averaging of temporal dynamical information and the subsequent loss of information. An analogy helps our point. Speech researchers have understood many years ago that speech is a locally stationary signal. As such, speech quantification is limited to windows in time where the signal is relatively stationary (10 msec windows). If we would use long term statistics to quantify speech, then all the local information would be washed away. Likewise, in brain dynamics, the dynamical measures should not be computed over long time intervals assuming stationarity as required by the dynamical theory of autonomous systems. We believe that this point is one of the distinguishing characteristics of our methodology and one of the pillars of its success.

The paper is organized as follows: We start by a brief description of the short-term largest Lyapunov exponent (STL_{max}), the nonlinear dynamical measure utilized in our research. We then apply the STL algorithm to EEG tracings, recorded from several brain sites, to create a set of STL_{max} time series containing local (in time and in space) information about dynamical mixing in the brain. We further create and quantify spatial maps of STL_{max} time series. At this level of analysis we are quantifying the brain spatio-temporal dynamics. We will show that it is at this level of analysis that reliable predictive measures of epileptic seizures are being derived.

II- Methods for Nonlinear Dynamical Analysis

II.1. Application to the EEG

The standard methods for time series analysis (e.g., power analysis, linear orthogonal transforms, parametric linear modeling) not only fail to detect the critical features of a time series generated by a nonlinear system, but may falsely suggest that most of the series is random noise [15]. In recent years, the methods developed for the dynamical analysis of complex series have been applied to the investigation of signals produced by real biological systems, such as the EEG. The EEG can be conceptualized as a series of numerical values (voltages) over time. Such a series is called a "time series", and an example of EEG from different stages of an epileptic seizure is shown in *Figure 1*. The ictal stage starts at the seizure's onset and ends at the seizure's end. The preictal stage is the period preceding the seizure onset. The postictal stage is the period following the seizure end. The period between the postictal stage of one seizure and the preictal stage of the next seizure is called interictal stage.

The EEG, being the output of a multidimensional system, has statistical properties that depend on both time and space [16]. Components of the brain (neurons) are densely interconnected and the EEG recorded from one site is inherently related to the activity at other sites. This makes the EEG a multivariable time series. A well-established technique for visualizing the dynamical behavior of a multidimensional (multivariable) system is to generate a phase space portrait of the system. A phase space portrait is created by treating each time-dependent variable of the system as a component of a vector in a multidimensional space, usually called state or phase space of the system. Each vector in the phase space represents an instantaneous state of the system. These time-dependent vectors are plotted sequentially in the phase space to represent the evolution of the state of the system over time. For many systems, this graphic display creates an object confined over time to a sub-region of the phase space. Such sub-regions of the phase space are called "attractors." The geometrical properties of these attractors provide information about the global state of the system.

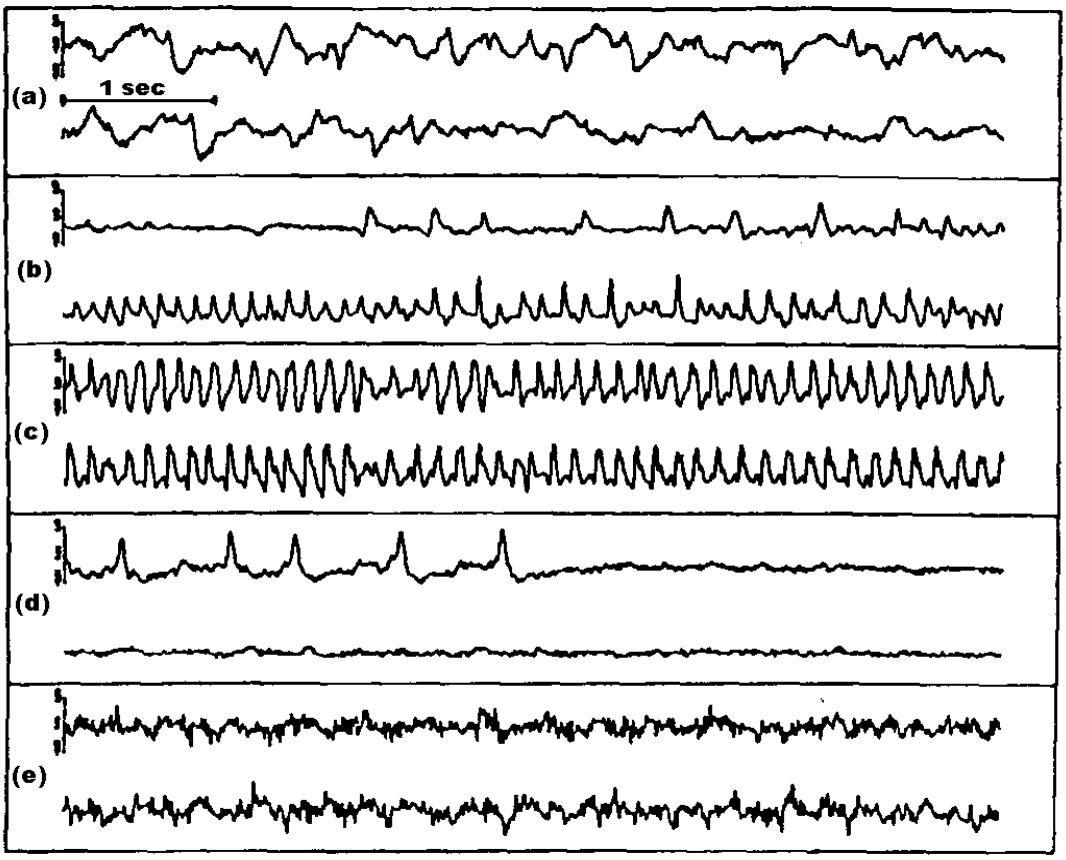

Figure 1: Five EEG segments from different stages of a human epileptic seizure (patient1) in the time domain (each segment is of 12 seconds duration and scaled separately). (a) preictal, (b) transition from preictal to ictal, (c) ictal, (d) transition from ictal to postictal, (e) postictal.

One of the problems in analyzing multidimensional systems is knowing which observable (variable of the system that can be measured) to analyze. In addition, experimental constraints may limit the number of observables that can be obtained. It turns out that when the variables of the system are related over time, which must be the case for a dynamical system to exist, proper analysis of a single observable can provide information about all variables of the system that are related to this observable. In principle, through the method of delays described by Packard et al. [17] and Takens [18], sampling of a single variable of a system over time can reproduce the related attractors of a system in the phase space. This technique for the reconstruction of the phase space from one observable can be used for the EEG. In *Figure 2b* a phase space portrait has been generated from an ictal EEG signal recorded by a single electrode located on the temporal cortex (*Figure 2a*). The characteristics of the formed epileptic attractor are typical for all of the seizures we have analyzed to date. This picture indicates the existence of limit

cycles in the phase space [1] (corresponding to periodic behavior in time domain) with trajectories moving in and out of the main body of the attractor (the large excursions correspond to spikes in time domain).

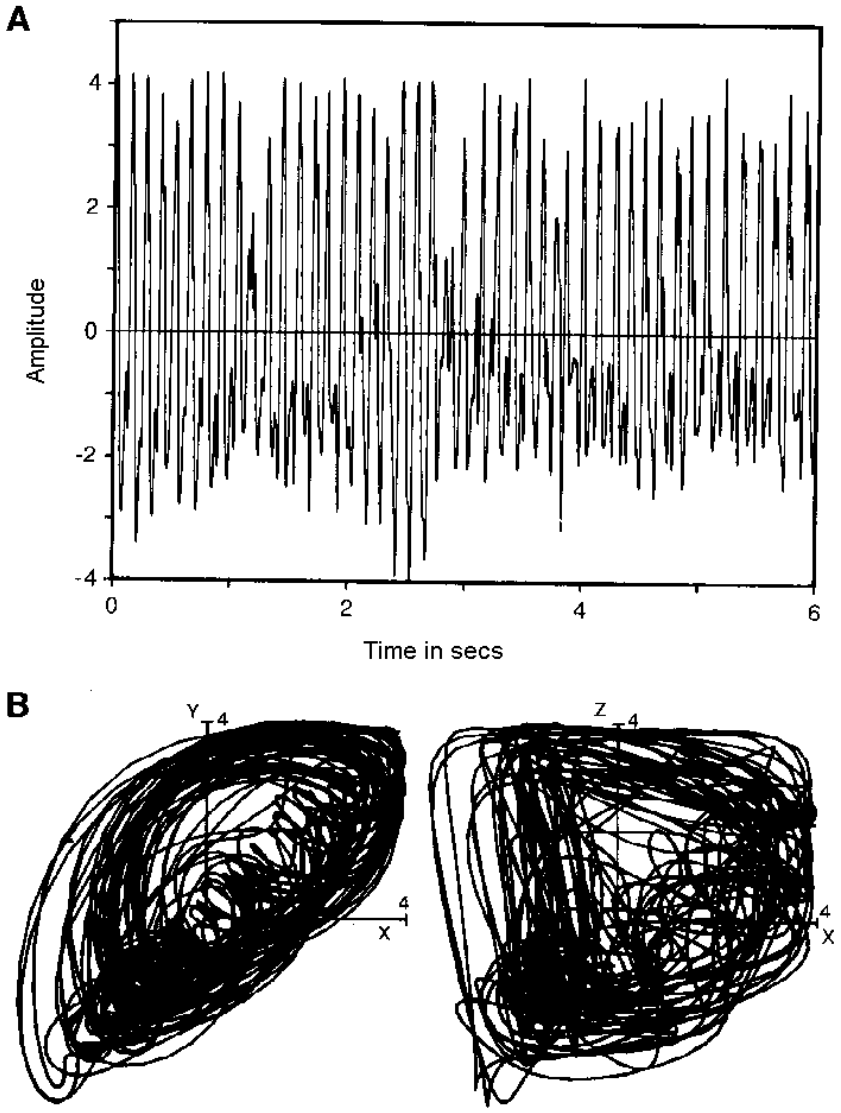

Figure 2: (a) Ictal segment of raw EEG data from an epileptic seizure (patient 1). (b) The EEG data in the phase space.

The geometrical properties of the phase portrait of a system can be expressed quantitatively using measures that ultimately reflect the dynamics of the system. For example, the complexity of an attractor is reflected in its dimension [19]. The larger the dimension of an attractor, the more complicated it appears in the phase space. It is important to distinguish between the dimension of the phase space (embedding dimension) and the dimension of the attractor. The embedding dimension (p) is the dimension of the phase space that contains the attractor and it is always a positive integer. On the other hand, the attractor dimension (D) may be a non-integer. D is directly related to the number of variables of the system and inversely related to the existing coupling among them.

According to Takens [18], the embedding dimension p should be at least equal to ($2*D + 1$) in order to correctly embed of an attractor in the phase space. Of the many different methods used to estimate D of an object in the phase space, each has its own practical problems [7, 19, 20]. The measure most often used to estimate D is the phase space correlation dimension (ν). Methods for calculating the correlation dimension from experimental data have been described [21, 22], and were employed in our work to approximate D of the epileptic attractor.

A chaotic attractor is an attractor where, on the average, orbits originating from similar initial conditions (nearby points in the phase space) diverge exponentially fast (expansion process); they stay close together only for a short time. If these orbits belong to an attractor of finite size, they will fold back into it as time evolves (folding process). The result of these two processes is a layered structure [14]. The measures that quantify the chaoticity of an attractor are the Kolmogorov entropy (K) and the Lyapunov exponents [23-25]. For an attractor to be chaotic, the Kolmogorov entropy or at least the maximum Lyapunov exponent (L_{max}) must be positive. The Kolmogorov (Sinai or metric) entropy (K) measures the uncertainty about the future state of the system in the phase space given information about its previous states (positions or vectors in the phase space). The Lyapunov exponents measure the average rate of expansion and folding that occurs along the local eigen-directions within an attractor in phase space. If the phase space is of p dimensions, we can estimate theoretically up to p Lyapunov exponents. However, only ($[D]+1$) of them will be real. The rest will be spurious [26]. Methods for calculating these dynamical measures from experimental data have been published [26-30]. The estimation of the largest Lyapunov exponent (L_{max}) in a chaotic system has been shown to be more reliable and reproducible than the estimation of the remaining exponents ([20], [31]), especially when D changes over time as it does with nonstationary data. We will now summarize our algorithm to estimate L_{max} from nonstationary data.

II.2. Estimation of Short Term Largest Lyapunov Exponents (STL_{max})

As we discussed in the introduction, a relevant time scale should always be used in order to quantify the physiological changes occurring in the brain. Furthermore, the brain being a nonstationary system, algorithms used to estimate measures of the brain dynamics

should be capable of automatically identifying and appropriately weighing existing transients in the data. The method we developed for estimation of STL_{max}, an estimate of L_{max} for nonstationary data, is explained in detail elsewhere [12, 27]. Herein we will present only a short description of our method.

Construction of the embedding phase space from a data segment $x(t)$ of duration T is made with the method of delays. The vectors X_i in the phase space are constructed as:

$$X_i = (x(t_i), x(t_i + \tau) \ldots . x(t_i + (p-1) * \tau))^T \quad (1)$$

where τ is the selected time lag between the components of each vector in the phase space, p is the selected dimension of the embedding phase space, and $t_i \in [1, T-(p-1)\tau]$. If we denote by L the estimate of the short term largest Lyapunov exponent STL_{max} then:

$$L = \frac{1}{N_a \Delta t} \sum_{i=1}^{N_a} \log_2 \frac{\left|\delta X_{i,j}(\Delta t)\right|}{\left|\delta X_{i,j}(0)\right|} \quad (2)$$

with

$$\delta X_{i,j}(0) = X(t_i) - X(t_j) \quad (3)$$

$$\delta X_{i,j}(\Delta t) = X(t_i + \Delta t) - X(t_j + \Delta t) \quad (4)$$

where:

- $X(t_i)$ is the point of the fiducial trajectory $\phi_t(X(t_o))$ with $t = t_i$, $X(t_o) = (x(t_o) \ldots x(t_o + (p - 1) * \tau))^T$, ^{T} denotes the transverse, and $X(t_j)$ is a properly chosen vector adjacent to $X(t_i)$ in the phase space (see below).

- $\delta X_{i,j}(0) = X(t_i) - X(t_j)$ is the displacement vector at t_i , that is, a perturbation of the fiducial orbit at t_i , and $\delta X_{i,j}(\Delta t) = X(t_i + \Delta t) - X(t_j + \Delta t)$ is the evolution of this perturbation after time Δt.

- $t_i = t_o + (i - 1) * \Delta t$ and $t_j = t_o + (j - 1) * \Delta t$, where:
  $i \in [1, N_a]$, and $j \in [1, N]$ with $j \neq I$

- Δt is the evolution time for $\delta X_{i,j}$, that is, the time one allows $\delta X_{i,j}$ to evolve in the phase space. If the evolution time Δt is given in *sec*, then L is in *bit/sec*.

- t_o is the initial time point of the fiducial trajectory and coincides with the time point of the first data in the data segment of analysis. In the estimation of L, for a complete scan of the attractor, t_o should move within $[0, \Delta t]$.

- N_a is the number of local L_{max}'s that will be estimated within a duration T data segment. Therefore, if Dt is the sampling period of the time domain data, $T = (N - 1)*Dt = N_a * \Delta t + (p - 1) * \tau$.

The short term largest Lyapunov exponent STL_{max} is computed by a modified version of the program proposed by Wolf et a*l.* [27]. We call the measure short term to differentiate it from the ones in autonomous dynamical systems studies. We found that for small data segments with transients, as in epileptic data, a modification of this algorithm is absolutely necessary for a better estimation of STL_{max}. This modification has to be made mainly in the searching procedure for a replacement vector at each point of a fiducial trajectory. For example, in our analysis of the EEG, we found that the crucial parameter of the L_{max} estimation procedure, in order to distinguish between the preictal, the ictal and the postictal stages, was not the evolution time Δt nor the angular separation $V_{i,j}$ between the evolved displacement vector $\delta X_{i-1,j}(\Delta t)$ and the candidate displacement vector $\delta X_{i,j}(0)$ (as it was claimed in Frank et al. [32]). The crucial parameter is *the adaptive estimation in time and phase space of the magnitude bounds* of the candidate displacement vector (see *Eq. 8* below) to avoid catastrophic replacements. Results from simulation data of known attractors have shown the improvement in the estimates of L achieved by using the proposed modifications [11].

Our rules can be stated as follows:

- For L to be a reliable estimate of STL_{max} , the candidate vector $X(t_j)$ should be chosen such that the previously evolved displacement vector $\delta X_{(i-1),j}(\Delta t)$ is almost parallel to the candidate displacement vector $\delta X_{i,j}(0)$, that is,

  $$|V_{i,j}| = |< \delta X_{i,j}(0), \delta X_{(i-1),j}(\Delta t) >| \leq V_{max} \qquad (5)$$

  where V_{max} should be small and $|< \varepsilon, \phi >|$ denotes the absolute value of the angular separation between two vectors ε and ϕ in the phase space.

- For L to be a reliable estimate of STL_{max} , $\delta X_{i,j}(0)$ should also be small in magnitude in order to avoid computer overflow in the future evolution within very chaotic regions and to reduce the probability of starting up with points on separatrices [33]. This means,

  $$|\delta X_{i,j}(0)| = |X(t_i) - X(t_j)| < \Delta_{max} \qquad (6)$$

  with Δ_{max} assuming small values.

Therefore, the parameters to be selected for the estimation procedure of L are:

- the embedding dimension p and the time lag τ for the reconstruction of the phase space
- the evolution time Δt (number of iterations N_a)
- the parameters for the selection of $X(t_j)$, that is, $V_{i,j}$ and Δ_{max}

- the duration of the data segment T

It is worth noting here that since only vector differences are involved in the estimation of L (*Eq. 2*), any DC present in the data segment of interest does not influence the value of L. In addition, only vector difference ratios participate in the estimation of L. This means that also L is not influenced by the scaling of the data (as long as the parameters involved in the estimation procedure, i. e. Δ_{max} , do not assume absolute values but relative ones to the scale of every analyzed data segment). Both points above make sense when one recalls that L relates to the entropy rate of the data [30].

Selection of p and τ: We select p such that the dimension v of the attractor in phase space is clearly defined. In the case of the epileptic attractor [11, 28, 34], $v = 2 \sim 3$, and according to Takens Theorem a value of $p \geq (2* 3 + 1) = 7$ is adequate for the embedding of the epileptic attractor in the phase space. This value of p may be too small for the construction of a phase space that can embed all states of the brain interictally, but it should be adequate for detection of the transition of the brain toward the ictal stage if the epileptic attractor is active in its space prior to the occurrence of the epileptic seizure. The parameter τ should be as small as possible to capture the shortest change (i.e. highest frequency component) present in the data. Also, τ should be large enough to generate (with the method of delays) the maximum possible independence between the components of the vectors in the phase space. In the literature, these two conditions are usually addressed by selecting τ as the first minimum of the mutual information between the components of the vectors in the phase space or as the first zero of the time domain autocorrelation function of the data [26]. Theoretically, since the time span $(p\text{-}1)*\tau$ of each vector in the phase space represents the duration of a state of the system, $(p\text{-}1)*\tau$ should be at most equal to the period of the maximum (or dominant) frequency component in the data. For example, a sine wave (or a limit cycle) has v =1, then a p=2*1+1=3 is needed for the embedding and $(p\text{-}1)*\tau$ =2*τ should be equal to the period of the sine wave. Such a value of τ would then correspond to the Nyquist sampling of the sine wave in the time domain. In the case of the epileptic attractor, the highest frequency present is 70*Hz* (the EEG data are L.P. filtered at 70*Hz*), which means that if p=3, the maximum τ to be selected is about 7*msec*. However, since the dominant frequency of the epileptic attractor (i.e. during the ictal period) was never more than 12 Hz, according to the above reasoning, the adequate value of τ for the reconstruction of the phase space of the epileptic attractor is*:* $(7-1)*\tau$ =83 msec, that is, τ should be about 14msec (for more details see [12]).

Selection of Δt: The evolution time Δt should not be too large, otherwise the folding process within the attractor adversely influences L. On the other hand, it should not be too small, in order for $\delta X_{i,j}(\Delta t)$ to follow the direction of the maximum rate of information change. If there is a dominant frequency component f_0 in the data, Δt is usually chosen as $\Delta t = {}^1/_2\, f_0$. Then, according to the previous arguments for the selection of p and τ, the $\Delta t \approx ((p\text{-}1)*\tau)/2$, which for EEG results in $\Delta t \approx 42$*msec*. In [12], it is shown that such a value is

within the range of values for Δt that can very well distinguish the ictal from the preictal state.

Selection of V_{max}: It sets the limits for the variation of $V_{i,j}$. We start with an initial V_{max} *(initial) = 0.1rad*. In the case that a replacement vector $X(t_j)$ is not found with $0 \leq |V_{i,j}| < V_{max}$ *(initial)* and $|\delta X_{ij}(0)| < 0.1 * \Delta_{max}$, we relax the bound for $|\delta X_{ij}(0)|$ and repeat the process with bounds up to $0.5* \Delta_{max}$. If not successful, we relax the bounds for $|V_{i,j}|$ by doubling the value of V_{max} and repeat the process with bounds for V_{max} up to 1 *rad*. Values of V_{max} larger than *0.8rad* never occurred in the procedure. If they do, the replacement procedure stops, a local $L(t_i)$ is not estimated at t_i and we start the whole procedure at the next point in the fiducial trajectory.

Selection of Δ_{max}: In Wolf's algorithm, Δ_{max} is selected as

$$\Delta_{max} = \max_{j,\, i} |\delta X_{i,j}(0)| \qquad (7)$$

where $j = 1,\ldots, N$ and $i = 1,\ldots, N_a$.
Thus, Δ_{max} is the global maximum distance between any two vectors in the phase space of a segment of data. This works fine as long as the data are stationary and relatively uniformly distributed in the phase space. With real data this is hardly the case, especially with the brain electrical activity which is strongly nonstationary and nonuniform [35-37]. Therefore, a modification in the searching procedure for the appropriate $X(t_j)$ is essential. First, an adaptive estimation of Δ_{max} is made at each point $X(t_i)$, and the estimated variable is

$$\Delta_{i,max} = \max_{j} |\delta X_{i,j}(0)| \qquad (8)$$

where $j = 1,\ldots, N$. By estimating Δ_{max} as above, we take care of the nonuniformity of the phase space (Δ_{max} is now a spatially local quantity of the phase space at a point $X(t_i)$) but not of the effect of existing nonstationarities in the data. We have attempted to solve the problem of nonstationarities by estimating Δ_{max} also as a temporally local quantity. Then, a more appropriate definition for Δ_{max} is:

$$\Delta_{i,max} = \max_{\mathrm{IDIST}_1 < |t_i - t_j| < \mathrm{IDIST}_2} |\delta X_{i,j}(0)| \quad \text{with } j \neq i \qquad (9)$$

and

$$\mathrm{IDIST}_1 = \tau \qquad (10)$$

$$\mathrm{IDIST}_2 = (p - 1) * \tau \qquad (11)$$

where IDIST1 and IDIST2 are the upper and lower bounds for $|t_i - t_j|$, that is, for the temporal window of local search.
Thus, the search for $\Delta_{i,max}$ is always made temporally about the state $X(t_i)$ and its changes within a period of the time span $(p\text{-}1)*\tau$ of a state. According to the previous formulae, the values for the parameters involved in the adaptive estimation of

$\Delta_{i,max}$ in our EEG data are: $IDIST_1=\tau=$ 14msec and $IDIST_2=(p-1)*\tau=$ 84msec.

Selection of $X(t_j)$: The replacement vector $X(t_j)$ should be spatially close to $X(t_i)$ in phase space (with respect to magnitude and angle deviation), as well as temporally not very close to $X(t_i)$ to allow selecting $X(t_j)$ from a nearby (but not the same) trajectory (otherwise, by replacing one state with one that shares common components would lead to a false underestimation of L). The above two arguments are implemented in the following relations:

$$0 \le |V_{i,j}| < V_{i,j}\ (initial) = 0.1rad \quad (12)$$

$$b * \Delta_{i,max} \le \delta X_{i,j}(0) \le c * \Delta_{i,max} \quad (13)$$

$$|t_i - t_j| > IDIST_3 \approx (p-1) * \tau \quad (14)$$

The parameter c starts with a value of 0.1 and increases, with a step of 0.1, up to 0.5, in order to find a replacement vector $X(t_j)$ satisfying *Eq. 12* through *Eq. 14*. The parameter b must be smaller than c and is used to account for the possible noise contamination of the data, denoting the distance below which the estimation of L may be inaccurate (we have used b=0.05 for our data [12, 27]). The temporal bound $IDIST_2$ should not be confused with the temporal bound $IDIST_3$, since $IDIST_2$ is used to find the appropriate $\Delta_{i,max}$ at each point $X(t_i)$ (searching over a limited time interval), whereas $IDIST_3$ is used to find the appropriate $X(t_j)$ within a $\Delta_{i,max}$ distance from $X(t_i)$ (searching over all possible times t_j).

Selection of T: For data obtained from a stationary state of the system, the time duration T of the analyzed segment of data may be large for the estimate of L to converge to a final value. For nonstationary data we have two competing requirements: on one hand we want T to be as small as possible to provide local dynamic information, but on the other hand the algorithm requires a minimum length of the data segment to stabilize the estimate of STL_{max}. *Figure 3* shows a typical plot for the change of STL_{max} with the size of the window for segments in the preictal and ictal stage of a seizure. From this figure, it is clear that values of 10 to 12 seconds for T are adequate to distinguish between the two extreme cases (preictal and ictal) in our data and for the algorithm to converge.

After extensive sensitivity studies with EEG data in epilepsy [11, 12] we have concluded that the critical parameter of the algorithm just presented is the $IDIST_2$, that is the parameter that establishes a neighborhood in time at each point in fiducial trajectory for the estimation of the parameter $\Delta_{i,max}$, which then establishes a spatial neighborhood for this point in the phase space (see *Eq. 9*). This is very clearly illustrated in *Figure 4*. It is obvious that, with values of $IDIST_2$ greater than 160msec, one is not even able to distinguish between the preictal and the ictal state of a seizure based on the thus generated values of L!

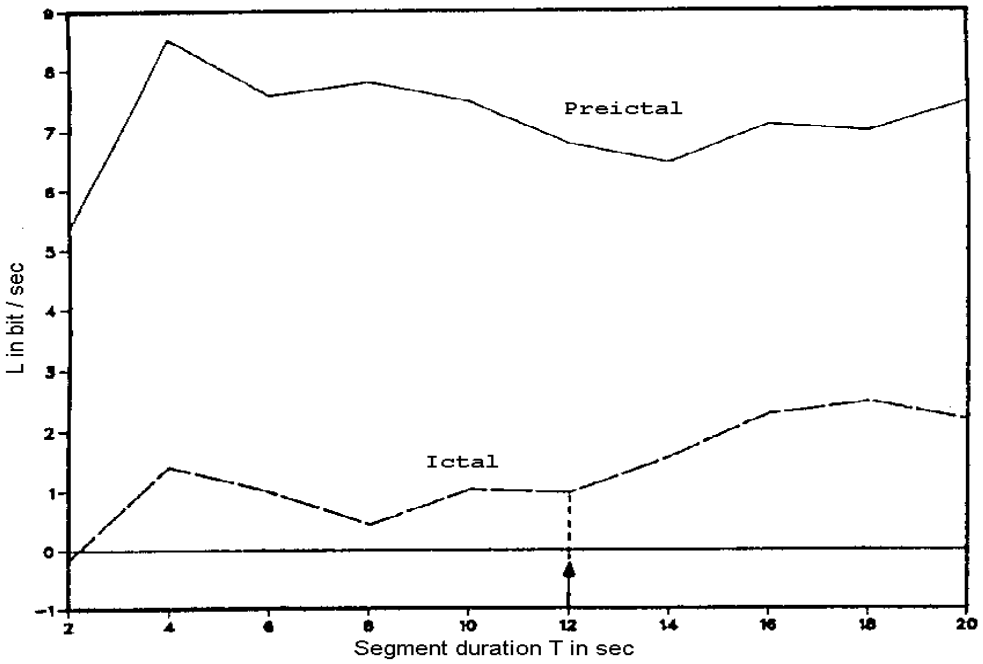

Figure 3: The variation of STL_{max} with the length T of the data segment for data in the preictal and ictal state of an epileptic seizure (patient 1). The rest of the parameters for the STL_{max} algorithm were: p=7, τ=14msec, Δt=42 msec, $IDIST_1$=14msec, $IDIST_2$=84msec, $IDIST_3$=84msec, b=0.05, c=0.1, $V_i j$ (initial)=0.1 rad..

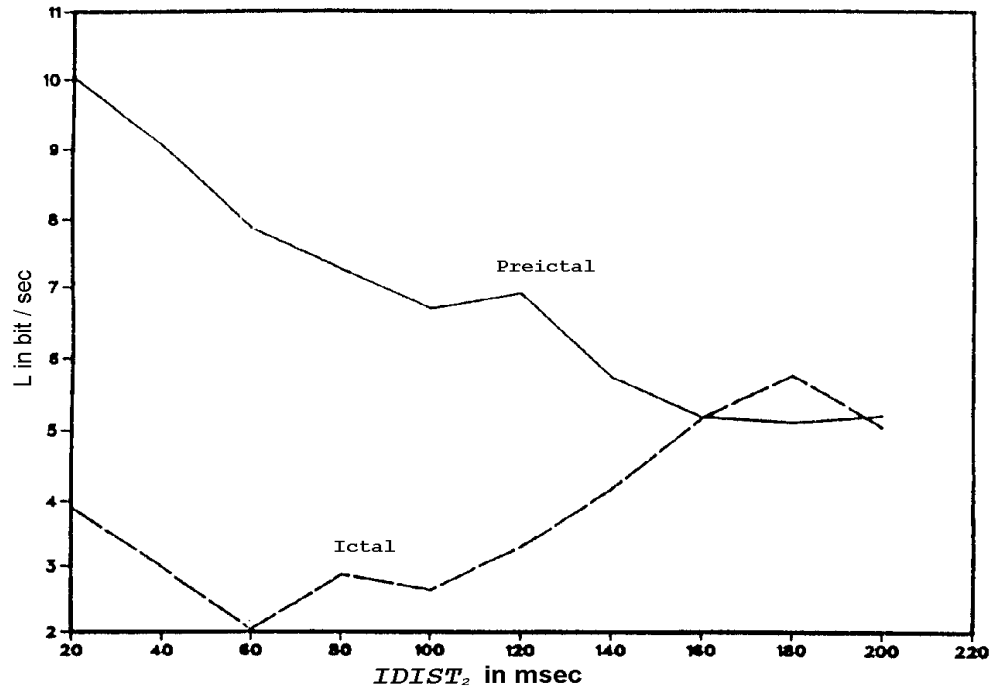

Figure 4: The variation of STL_{max} with the $IDIST_2$ parameter for data in the preictal and ictal state of an epileptic seizure (patient 1). The rest of the parameters for the STL_{max} algorithm were: p=7, τ=14msec, Δt=42 msec, $IDIST_1$=14msec, $IDIST_3$=84msec, b=0.05, c=0.1, $V_i j$ (initial)=0.1 rad.

III- STL_{max} time series of EEG data

We will now show the results of the application of our STL_{max} algorithm over time from long electrocorticographic (ECoG) and scalp EEG data. Our studies have employed recordings obtained from implanted electrodes placed in the hippocampus and over the inferior temporal and orbitofrontal cortex (ECoG), as well as coverage of the temporal lobes by a limited number of scalp electrodes (scalp EEG). *Figure 5* shows our typical 28 electrode montage used for subdural and depth recordings. Continuous EEG signals were typically analyzed for 1 hour before to 1 hour after a seizure, sampled with a sampling frequency of 256 Hz and low-pass filtered at 70 Hz. *Figure 6* depicts a typical ictal EEG recording, as manifested in scalp and depth electrodes, centered at the time of seizure onset.

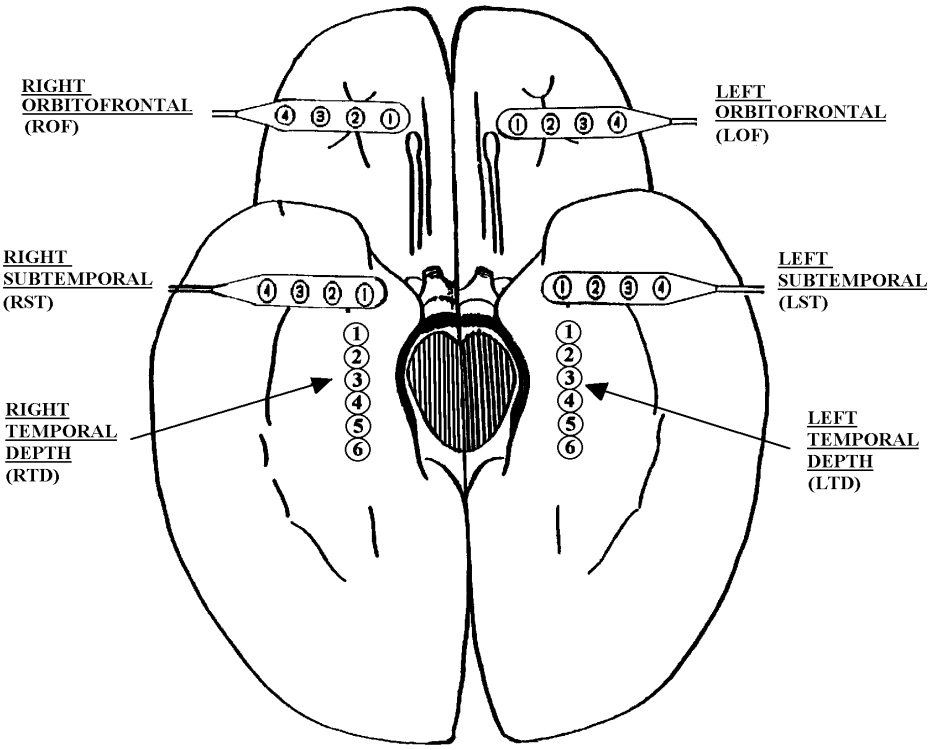

Figure 5. Schematic diagram of the depth and subdural electrode placement. This view from the inferior aspect of the brain shows the approximate location of depth electrodes, oriented along the anterior-posterior plane in the hippocampi (RTD - right temporal depth, LTD - left temporal depth), and subdural electrodes located beneath the orbitofrontal and subtemporal cortical surfaces (ROF - right orbitofrontal, LOF - left orbitofrontal, RST- right subtemporal, LST- left subtemporal).

Figure 6. A 13.6 sec EEG segment at the onset of a left temporal lobe seizure (patient 2), recorded referentially to linked ears from bilaterally placed depth (hippocampal) electrodes (first 11 channels; nomenclature according to Figure 5), sphenoidal electrodes (last 2 channels) and scalp electrodes (remaining 19 channels; nomenclature according to AEEGS guidelines for scalp recordings - extended International 10-20 System). The ictal discharge begins in the left depth electrodes (LTD 1-4) as a series of high frequency repetitive spikes, approximately 5 sec into the record. The initial manifestation of the seizure in scalp/sphenoidal electrodes is a diffuse drop in voltage, and a definitive ictal discharge approximately 6 seconds after the initial ictal discharge in the left hippocampus. The ictal discharge spreads to the right hippocampus about 13 seconds later (not shown in this figure).

By dividing the recorded EEG data from an electrode site into non-overlapping segments, each 12*sec* in duration, and estimating *L* from each of the thus created data segments, a profile of *L* over time per electrode site was generated. A typical plot of *L* over time, from the preictal to the postictal state of a seizure is shown in *Figure 7*. The exponent *L* is positive during the whole period of 19 minutes (10 minutes preictally, 2 minutes ictally and 7 minutes postictally). We can see that, even during the seizure where *L* assumes its lowest value (the seizure can easily be detected from the lowest values of *L), L* is still positive. This is consistent with an interpretation of the ictal stage as a stage of fewer degrees of freedom than before, usually enough for the system to find a way out and the patient to recover [38]. Comparing the mean value of *L* in the preictal state with the one in the postictal state, we can deduce that the preictal state is less chaotic than the immediate postictal one. The seizure's onset corresponds to the maximum drop in the values of L that were obtained at electrodes participating in the manifestation of the seizure. This was typical for all analyzed seizures across our subjects. Also, in the preictal state of Figure 7, one can notice two prominent drops in the values of *L*, one about 150*sec* and the other 450*sec* into the record. These preictal drops in *L* can be explained as attempts of the system toward a phase transition much before (minutes) the actual seizure

outburst. Such an explanation, as well as the answer to why the seizure did not occur at these preictal points but much later, required the consideration of the activity at other electrode sites as well.

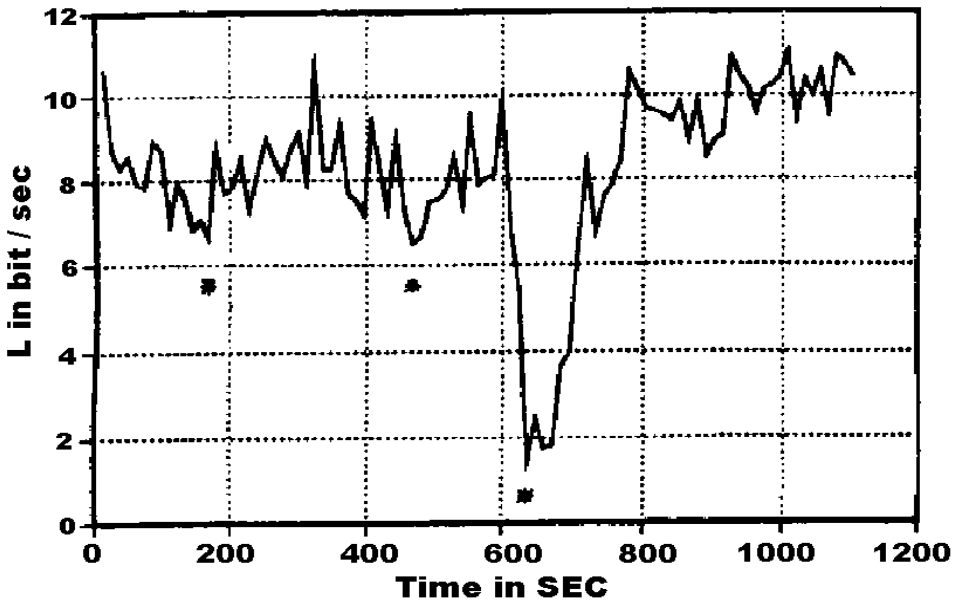

Figure 7: Plot of the STL_{max} over time derived from an EEG signal recorded at an electrode site not overlying the seizure focus (patient 1). The estimation of the L values was made by dividing the signal into non-overlapping segments of 12sec each.

In *Figure 8a*, we present the Lyapunov profile of the EEG recorded from an electrode site overlying the seizure focus for the same seizure as in Figure 6. We notice here that a prominent preictal drop in *L* occurs 350*sec* into the record. We also notice that the preictal profile thereafter (segment *A*: 350*sec* to 600*sec* in the record) is very similar in morphology to the immediate postictal profile (segment *B:* 700*sec* to 1000*sec* in the record), the latter being more dilated. This becomes clear in *Figure 8b*, where the crosscorrelation of segment *B* with the entire Lyapunov profile is shown. The global maximum of this crosscorrelation occurs at about *720sec* (approximately the starting point of segment B), as it was expected. In addition, we notice a prominent local maximum of the crosscorrelation in the preictal period at about 350*sec*, a time lag that corresponds to the beginning of the preictal segment *A*. This suggests that *A* and *B* are strongly correlated, and it indicates that the brain exhibits cyclic behavior going into and out of the phase transition. This behavior was invisible from the raw EEG data or from the clinical symptoms of the patient before and after the seizure.

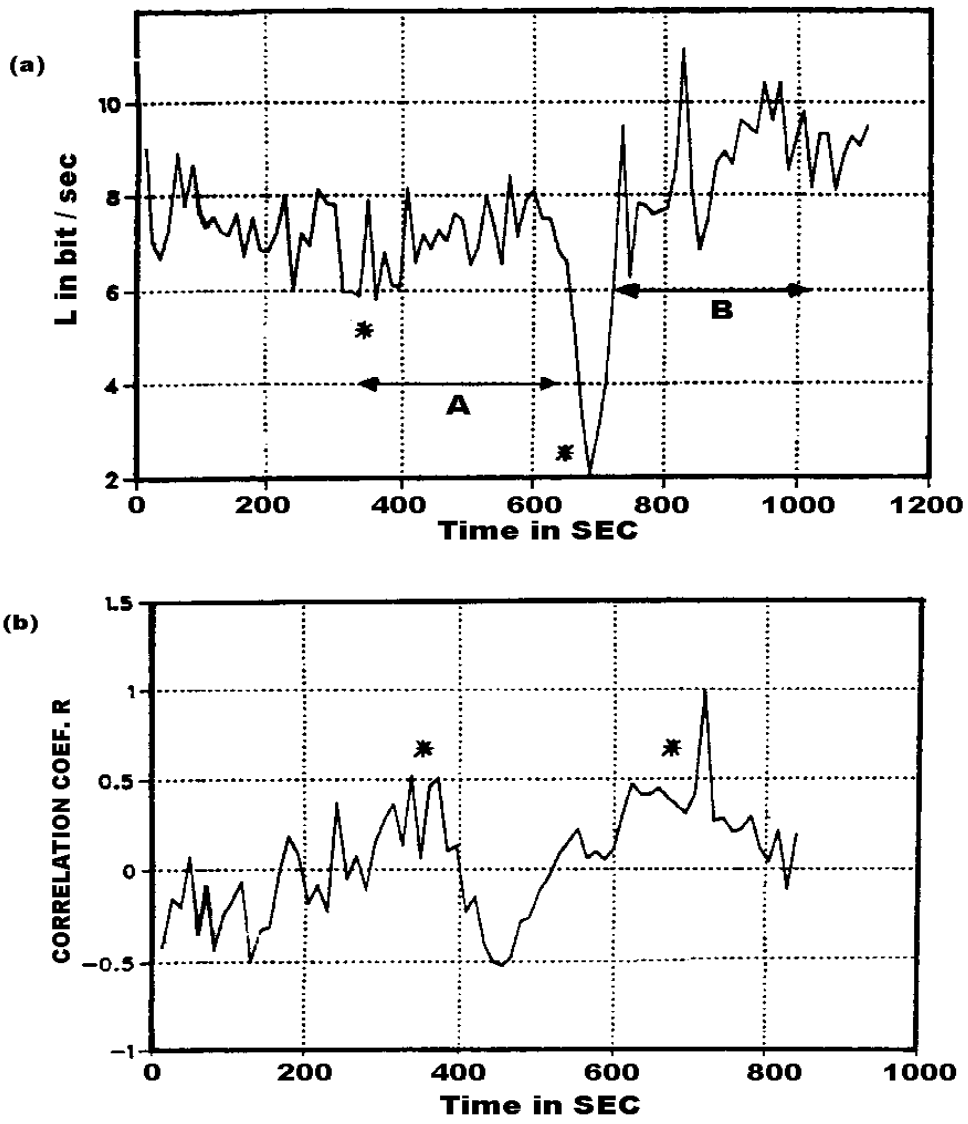

N

Figure 8: (a) Plot of the Lyapunov exponent over time derived from an EEG signal recorded at an electrode site overlying the seizure focus (patienr 1). (b) Crosscorrelation of the postictal portion B of the STL_{max} in (a) with the entire record of STL_{max} in (a), after subtraction of the running mean of L.

In all cases studied to date, the largest drop in the value of the STL_{max} exponent occurred first at electrode sites located where the seizure discharge originated. Also, the chaoticity of the EEG signal (reflected by the value of STL_{max}) was highest during the postictal state, lowest during the seizure discharge, and intermediate in the preictal state. Thus, from a dynamical perspective, the onset of a seizure represents a temporal transition of our system from a chaotic state to a less chaotic one (more ordered, corresponding to the synchronized rhythmic firing pattern of neurons participating in the seizure discharge) and back to a more chaotic state. In the next section we will show that this transition is mainly a spatio-temporal chaotic transition.

IV- Spatio-Temporal STL_{max} profiles

We will now present STL_{max} data preceding, during and following an epileptic seizure at various brain sites to illustrate the spatio-temporal dynamics involved in the manifestation of a seizure. The raw EEG data from each electrode site were divided into nonoverlapping segments of 12sec duration each. From each segment, the phase space was reconstructed and the maximum Lyapunov exponent was estimated with the algorithm described in section II. Thus, for each electrode site, profiles consisting of the values of STL_{max} over time were generated.

Preictal fluctuations in the value of L_{max} over time were observed at each recording site. Initially, the fluctuations among sites are out of phase and differ in their mean values. Beginning tens of minutes prior to a seizure, the mean values and phases of L_{max} at these sites start to converge. Several minutes prior to the seizure, there is a widespread locking among the STL_{max} estimates (both in value and phase) from different cortical regions in both sides of the brain. Seconds prior to seizure onset, STL_{max} values from most of the sampled regions of the brain are locked in an abrupt transition to a more ordered state. An example of such a situation is illustrated in *Figures 9* and *10*.

In Figure 9, the epileptic seizure occurred 46 minutes into the recording (the EEG profile of this seizure's onset is depicted in Figure 6). Locking between areas that overly the epileptogenic focus (left temporal lobe in this patient) may exist for a long time prior to a seizure. For example, the locking of the left sphenoidal electrode (MN1) with the left fronto-temporal scalp electrode (FT9) was maintained for at least 46 minutes prior to the seizure (see Figure 9a). The locking of MN1 with the left hippocampus (LTD3) comes 21 minutes after its locking with the left fronto-temporal lobe (FT9) (see Figure 9b). Such long term dynamical interactions, revealed from analysis of the EEG, have never been reported in the EEG literature. Figure 10 shows the development of long term preictal locking of sites even across hemispheres: the epileptogenic left hippocampus with normal contralateral hippocampus (locked 10 minutes prior to seizure's onset - see Figure 10a), and the scalp electrode sites ipsilateral to the focus with homologous contralateral scalp electrode sites (locked 8 minutes prior to seizure's onset - see Figure 10b).

From the above, it is clear that the time of onset of locking among different sites may vary widely. For example, while the intra-hemispheric locking ipsilateral to the focus could be detected as long as 45 minutes prior to this seizure (see Figure 9a) the inter-hemispheric locking (e.g. between left and right hippocampus) does not start until 10 minutes prior to the seizure (see Figure 10a). Another relevant point is of note here: although a 10 minute preictal locking between the hippocampi is evident from our analysis of the EEG, interaction of the two hippocampi is visually detectable in the raw EEG only 13 second after the seizure's onset (see Figure 6). We will return to this important point later in this section.

Four important characteristics of the locking process prior to an epileptic seizure can now be inferred. All these characteristics have regularly been observed in our analyses with depth and subdural electrodes and appear to be also detected with scalp recordings. The **first characteristic** is that a pair of sites may be locked for some period of time and subsequently may become unlocked without occurrence of a clinical seizure. For example, in Figure 10a, the left hippocampus locked with the right hippocampus about 18

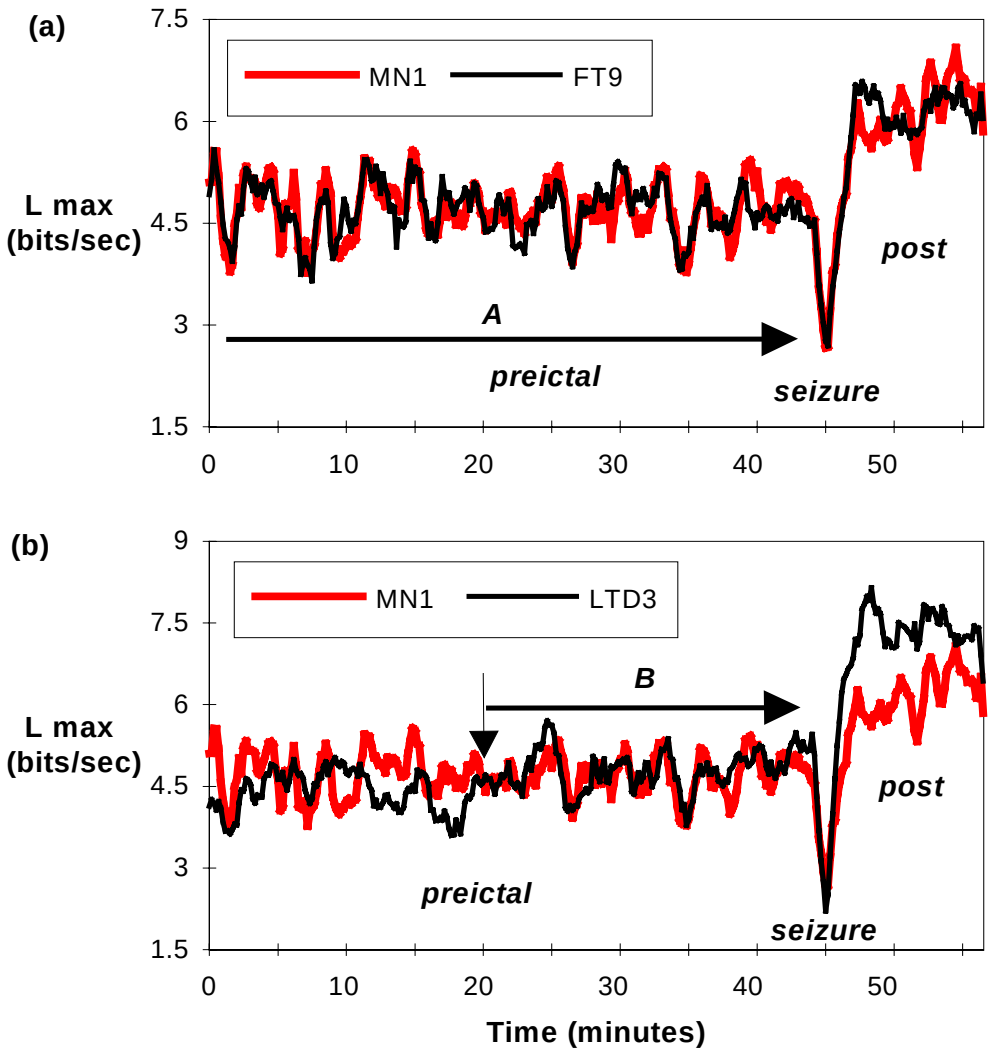

Figure 9. Locking within the epileptogenic left temporal lobe. The seizure's onset is at 46 minutes into the recording and it is depicted in Figure 6. The patient was awake and this seizure lasted for 1.8 minutes (patient 2). (a) Sphenoidal (MN1) vs. frontotemporal scalp (FT9): the mean values of L_{max} remain similar throughout the entire preictal trace (period A). The seizure is characterized by a simultaneous drop in the value of L_{max} in both electrodes. (b) Sphenoidal (MN1) vs. left hippocampus (LTD3): the L_{max} profiles become value and phase entrained 25 minutes prior to seizure, remain locked until the seizure (period B), and are unlocked postictally.

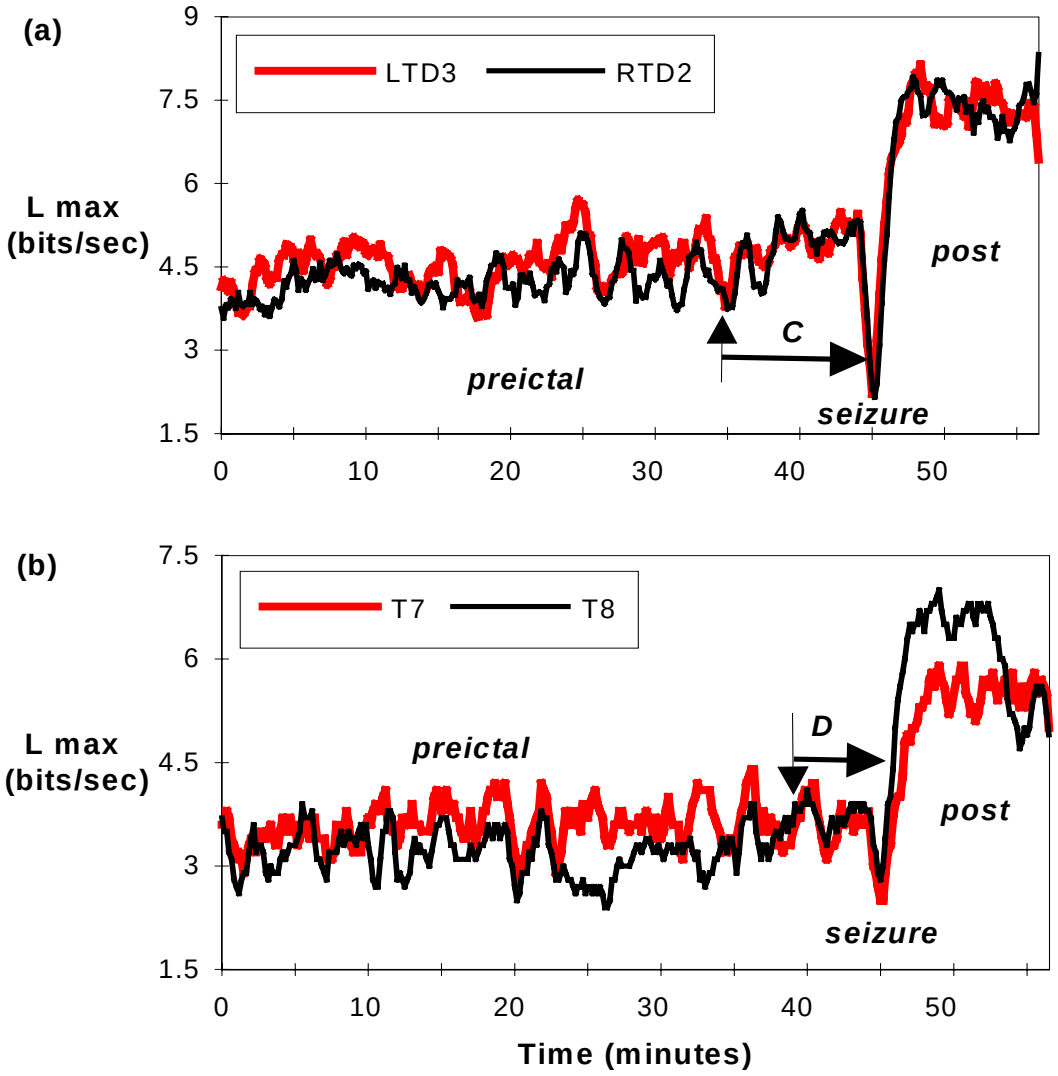

Figure 10. Locking of the epileptogenic left temporal lobe with homologous contralateral sites. The seizure's onset is at 46 minutes into the recording and it is depicted in Figure 6. The patient was awake and this seizure lasted for 1.8 minutes (patient 2). (a) Long-term locking between the left and right hippocampus for approximately 10 minutes prior to seizure (period C). (b) Long-term locking between the left (T7) and right temporal (T8) scalp electrode sites for approximately 8 minutes prior to seizure (period D).

and 26 minutes into the recording and then unlocked until 35 minutes into the recording, thereafter remaining locked up to the occurrence of the seizure (period C). The **second characteristic** is that a number of critical sites have to be locked with the epileptogenic focus over a common period of time in order for a seizure to take place. This forms the basis of our critical mass hypothesis. From Figures 9 and 10, it is clear that the order of preictal locking intervals for the analyzed seizure in this patient was: A→B→C→D, that is, left temporal cortex with left frontotemporal cortex (MN1-FT9) → left temporal

cortex with left hippocampus (MN1-LTD3) → left hippocampus with right hippocampus (LTD3-RTD2) → left temporal cortex with right temporal cortex (T7-T8). The **third characteristic** is the progressiveness and the large time constants involved in the process of locking of brain sites. The **fourth characteristic** is the postictal resetting of the brain. It appears that epileptic seizures occur only under abnormal conditions of increased spatio-temporal order in the brain. It also appears that the seizure itself represents a resetting of the brain from the preictal, abnormal, state to a reduced spatio-temporal order, more normal, state. This theory of resetting is supported by our observations from the spatio-temporal preictal locking and the spatiotemporal postictal unlocking with the epileptogenic focus of STL_{max} profiles of various brain sites.

IV.2. Quantification of the Spatio-Temporal Dynamics

We will now examine the spatio-temporal dynamical changes in the EEG prior to, during and after epileptic seizures, by quantifying the observed progressive locking and unlocking of STL_{max} profiles over time and space. We employ the *T*-index (from the well-known *t*-test for comparisons of means of paired –dependent- observations) as a measure of distance between the mean values of pairs of STL_{max} profiles over time. The *T*- index at time *t* between electrode sites *i* and *j* is then defined as:

$$T_{i,j}(t) = \mathrm{E}\{\,|\,STL_{max,i}(t) - STL_{max,j}(t)\,|\,\} \div \frac{\sigma_{i,j}(t)}{\sqrt{N}} \qquad (15)$$

where E{ } denotes the average of all absolute differences $|\,STL_{max,i}(t) - STL_{max,j}(t)\,|$ within a moving window $w_t(\lambda)$ defined as:

$$w_t(\lambda)=1 \text{ for } \lambda \in [\,t\text{-}N\text{-}1,\, t\,] \text{ and } w_t(\lambda)=0 \text{ for } \lambda \notin [\,t\text{-}N\text{-}1,\, t\,]$$

where *N* is the length of the moving window. Then, $\sigma_{i,j}(t)$ is the sample standard deviation of the STL_{max} differences between electrode sites *i* and *j* within the moving window $w_t(\lambda)$. The thus defined *T*-index follows a t-distribution with N-1 degrees of freedom.

In the estimation of the $T_{i,j}(t)$ indices in our data we used N=30 (i.e. averages of 30 differences of STL_{max} exponents per moving window and pair of electrode sites). Since each exponent in the STL_{max} profiles is derived from a 12 second EEG data segment, the length of the window used corresponds to approximately 6 minutes in real time units. Therefore, a two-tailed t-test with N-1=29 degrees of freedom, at a statictical significance level α, should be used to test the null Hypothesis Ho = 'brain sites *i* and *j* acquire identical STL_{max} values at time *t*'. If we set α=0.1, the probability of a type I error, or better, the probability of falsely rejecting Ho if Ho is true, is 10%. For the *T*-index to pass this test $T_{i,j}(t)$ should be less than 1.699.

We will show the results of such an analysis through an example. In *Figure 11*, the EEG of a seizure onset is depicted from a patient with an epileptogenic focus in the left

hippocampus. Electrode site LTD2 in the left hippocampus appears to show the ictal onset prior to all other sites. Within seconds the discharge spreads to electrode sites in both hemispheres. No visual signs of the impending seizure from the EEG are present before the appearance of the initial discharge at LTD2. We will now show that this EEG picture is not fully representative of what is really occurring.

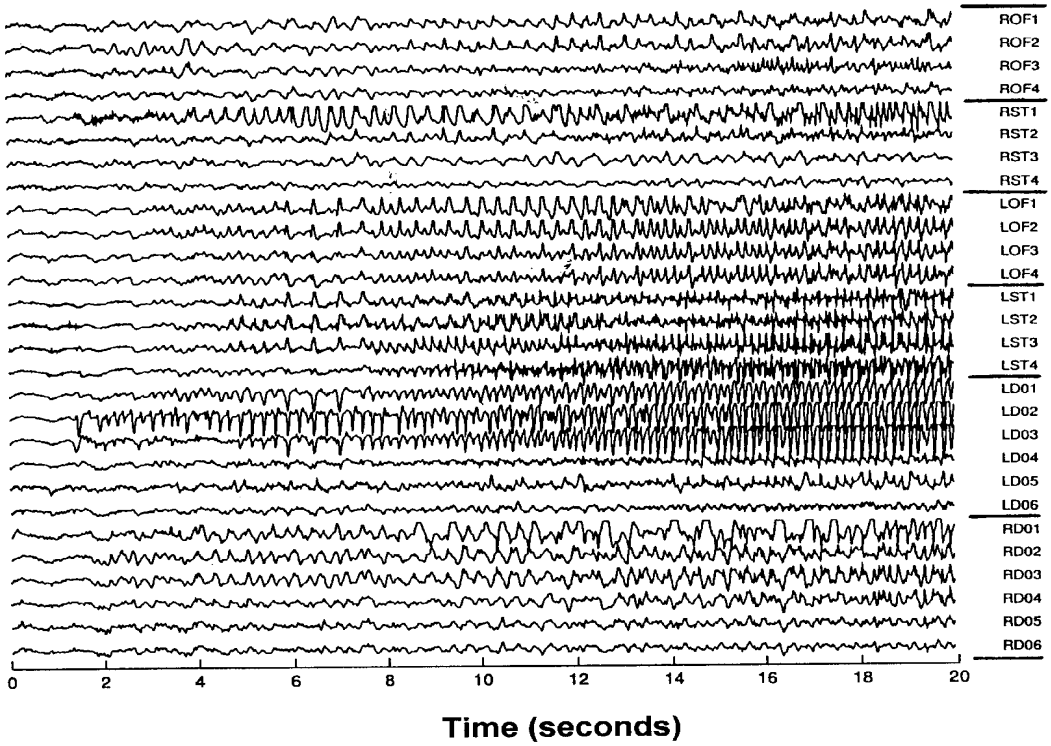

Figure 11. A 20 sec EEG segment at the onset of a left temporal lobe seizure (patient 3), recorded referentially to linked ears from bilaterally placed 12 depth (hippocampal) electrodes (last 12 channels in the figure), 8 subdural temporal electrodes and 8 subdural orbitofrontal electrodes (nomenclature according to Figure 5). The ictal discharge begins as a series of high amplitude sharp and slow wave complexes in the left depth electrodes (LTD 1-3, more prominently LTD2) approximately 1.5 sec into the record. Within seconds, it spreads to RST1, the right hippocampus (RTD1-3), the left temporal and frontal lobe. It lasts for 80 seconds (not shown in this figure).

We first visually examine the STL_{max} profiles in *Figure 12* generated from our analysis of the EEG at 7 electrode sites representing all 6 recording areas (LTD1 and LTD3 from the epileptogenic left hippocampus, RTD2 from the more normal right hippocampus, LST4 from the surface of the left temporal cortex, RST4 from the surface of the right temporal cortex, LOF3 from the surface of the left orbitofrontal cortex, ROF3 from the surface of the right orbitofrontal cortex). We see that: a) the LTD1 and LTD3 from the epileptogenic left hippocampus exhibit similar preictal entropy rates ($STL_{max)}$, being

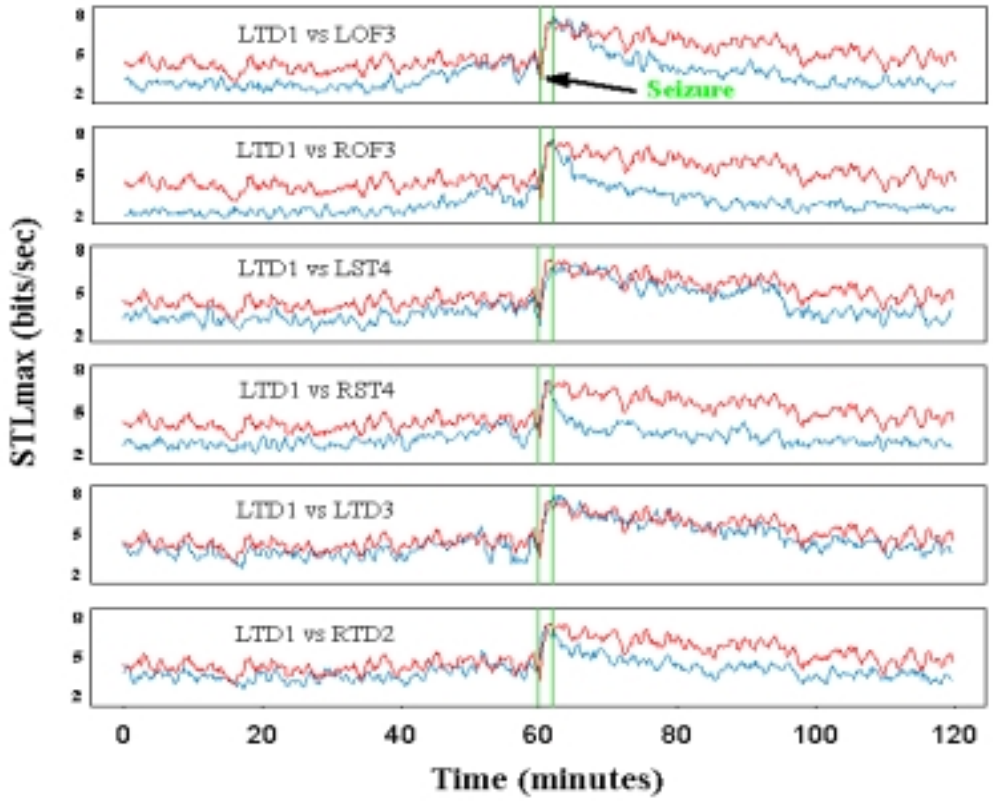

Figure 12. Preictal locking and postictal unlocking of the epileptogenic left hippocampal site LTD1 to sites from the rest of the recording areas. Pairs of 5-point smoothed STL_{max} profiles from LTD1 and one electrode site per recording area are shown. The seizure onset was depicted in Figure 11 (patient 3) and it is located 60 minutes into the record shown here, corresponding to the maximum drop of the unsmoothed STL_{max} values at LTD1 and LTD2. Although the seizure's duration was only 80 seconds, in this figure it is denoted as 1 minute and 80 seconds (time between the vertical green lines) since this is the time the seizure itself influences the STL_{max} values due to its duration and the 1 minute moving average smoothing of the STL_{max} profiles. The most prominent preictal locking is observed within the epileptogenic hippocampus as well as between the epileptogenic and contralateral hippocampi. The rest of the recording areas lock to the epileptogenic hippocampus in the last 5 minutes prior to seizure's onset. Postictally, the areas in the contralateral hemisphere (RTD, RST, ROF) unlock from the epileptogenic focus first. The areas in the ipsilateral hemisphere unlock from the epileptogenic focus last (LST, LOF).

more or less locked for 60 minutes prior to this seizure onset and start converging more at about 20 minutes prior to seizure onset. Postictally, this is the last pair to start unlocking, about 22 minutes after seizure ends. b) LTD1 and RTD2 exhibit similar entropy rates and start converging more about 8 minutes prior to seizure onset. Postictally, they unlock by seizure end. c) LST4 starts progressively locking to LTD1 about 20 minutes prior to seizure onset and finally locks to it about 5 minutes prior to seizure onset. Postictally, they start unlocking about 10 minutes after seizure end and are clearly unlocked 30 minutes after the seizure. d) RST4 starts progressively locking to LTD1 about 20 minutes prior to seizure onset and does not lock to it until the seizure onset. Postictally, they unlock by seizure end. e) LOF3 starts progressively locking to LTD1 about 20 minutes prior to seizure onset and finally locks to it about 5 minutes prior to seizure onset. Postictally, they start unlocking 3 minutes after seizure end. f) ROF3 starts progressively

locking to LTD1 about 20 minutes prior to seizure onset and does not lock to it until the seizure onset. Postictally, they unlock by seizure end.

The observations from the preictal and postictal STL_{max} profiles of the 6 pairs of the electrode sites we considered above are quantified with the T(t)-indices and presented in *Figure 13*. We can now order the pairs according to their preictal and postictal T-indices. From Figure 13 it is evident that, in this seizure, all recording areas exhibit preictal locking to the epileptogenic focus but differ in the degree and the timing of the initiation of the locking process. Preictally, the left and right hippocampi are the most strongly interacting areas (lowest value of T-index over time), left subtemporal cortex is the next strongly interacting area with the focus, right subtemporal cortex and left orbitofrontal are less strongly interacting with the focus, and finally, the right orbitofrontal area interacts the most weakly with the focus.

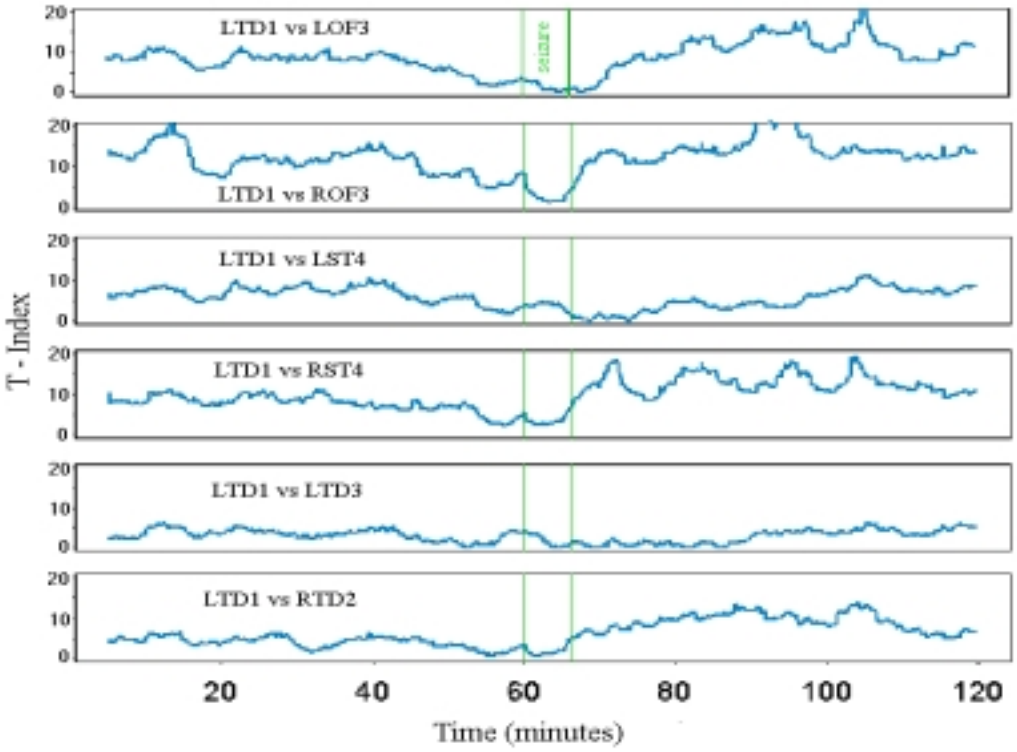

Figure 13. Quantification of the observed long-term locking in Figure 12 between the epileptogenic left hippocampus and ipsilateral as well as contralateral sites from all recording areas. Although the seizure duration was only 80 seconds, in this figure it is denoted as 7.4 minutes (time between the vertical green lines) since this is the time the seizure itself influences the STL_{max} values due to its duration and the 6 minute moving window for the estimation of the T-index profiles. The longest preictal and postictal locking (lowest values of T-index) is observed within the epileptogenic hippocampus (LTD1 vs. LTD3). The shortest preictal and postictal locking (highest values of T-index) is observed between the epileptogenic hippocampus (LTD1) and the contralateral orbitofrontal region of the cortex (ROF3).

Postictally, the most impressive observation is that all areas in the right, more normal,

hemisphere (RTD, RST, ROF) were the first to unlock (within seconds after the seizure) from the left epileptogenic hippocampus. The LOF area unlocks next (within 3 minutes from seizure's end). The two remaining areas, LST and LTD, are closer to the focus and are the last to unlock preictally from the focus (10 and 22 minutes respectively).

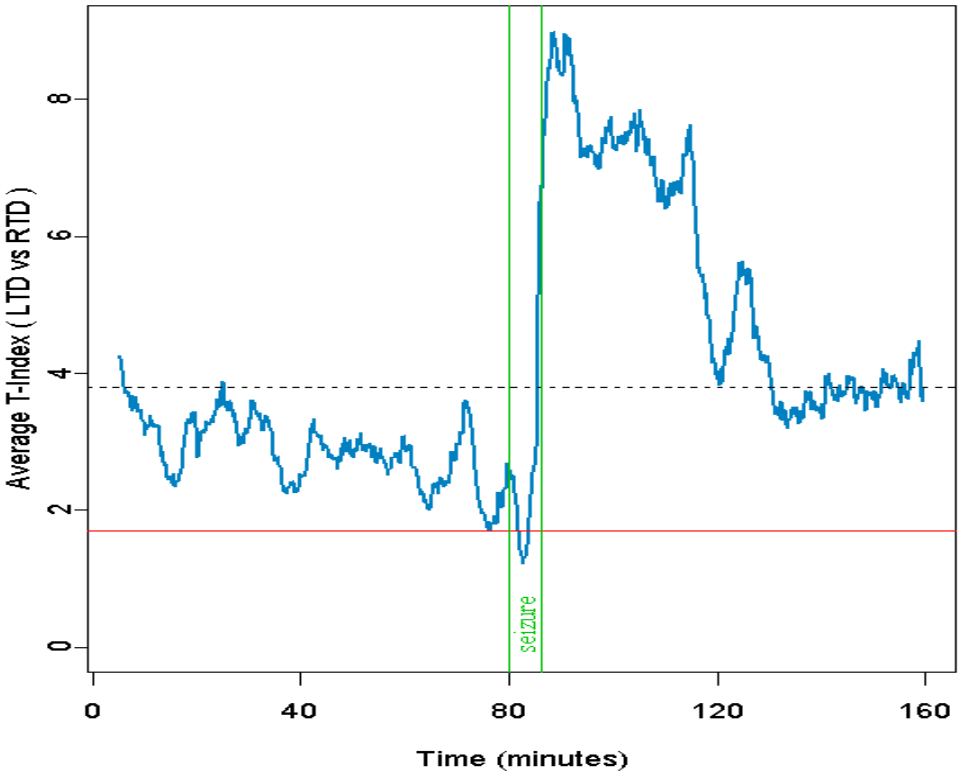

Figure 14. Average locking of all 6 electrode sites of the epileptogenic left hippocampus to the homologous 6 electrode sites of the more normal hippocampus. The seizure is the one depicted in Figure 11 (patient 3) and it is located 80 minutes into the record shown here. The average T-index of this interaction shows that onset of preictal locking precedes seizure's onset for at least 80 minutes. The red horizontal line denotes the value of the T-index that corresponds to the t-test's α=0.1 significance level. This line is approached by the preictal T-index values only a few minutes prior to seizure's onset and could be used as a threshold line for a short-term preictal prediction of this seizure. The dotted black horizontal line shows the postictal level of the T-index long after the end of the seizure (60 to 80 minutes). This line, in conjunction with the preictal average T-index values, could be used as a threshold line for a long-term preictal prediction of this seizure.

Finally, in *Figure 14*, we show that the spatiotemporal interaction during the preictal to ictal transition is even more striking when we consider larger groups of electrode sites. From Figures 12 and 13 we saw that (LTD1, RTD2) and (LTD1, LTD3) were the most closely locked electrode pairs preictally. It is interesting to see how the remaining pairs of electrode sites from the two hippocampi interact prior to this seizure. There are 36 pairs of interaction between the six LTD and the six RTD recording sites of each hippocampus.

In Figure 14 we present the average T-index profile estimated by averaging all 36 T-index profiles (one T-index profile per each electrode pair between the left and the right hippocampus). The important observation here is that, using the average T-index, we can detect a preictal transition (negative slope in the average T-index profile over an 80 minute preictal period) between the two hippocampi. That was not possible when we were considering pair interactions. For example, the preictal T-index for the pair (LTD1, RTD2) (depicted in Figure 13) hardly exhibits any negative slope over the 60 minute preictal period (exhibiting similar entropy rates and developing a warning for an impending seizure only 8 minutes prior to seizure onset). Group interactions may reveal a hidden global interaction or they may obscure a critical, local (i.e. pair) interaction. Identification of the critical electrode pair interactions is a challenging problem. While pair interactions can detect a critical local interaction, they may miss the global picture. (e.g. compare Figures 13 and 14).

The above findings indicate that the occurrence of an epileptic seizure represents a spatio-temporal phase transition involving widespread areas of the hippocampus and neocortex. This transition appears to occur over a much longer time scale than can be explained by current theories of epileptogenesis. However, these findings are quite consistent with the theories of synergetics and chaos. STL_{max} may well serve as one of the order parameters of the epileptic transition [39]. Further study is needed to identify and characterize control parameters that govern this transition.

V- Conclusions

The methodology for the estimation of STL_{max} profiles from the EEG (section II), quantification of the observed locking and unlocking of brain sites, as well as examples of the preictal locking and postictal unlocking (sections III and IV) were presented in this communication. By analyzing over time the STL_{max} values of EEG signals recorded from subdural electrodes placed over the epileptogenic temporal lobe and regions of ipsilateral frontal and parietal cortex, our group discovered that, beginning tens of minutes before seizure onset, regions of the anterior temporal cortex and regions more distant from the epileptogenic focus become locked with respect to their content of chaos. This observation indicated that, several minutes before a seizure, large regions of the cortex become dynamically locked as measured by the convergence of their STL_{max} profiles. The same locking process was subsequently demonstrated in recordings from hippocampal depth electrodes and scalp electrodes. After a seizure, there is a resetting of the preictal locking process.

Perhaps the most exciting discovery to emerge from dynamical analysis of the EEG in temporal lobe epilepsy is that human epileptic seizures are preceded by dynamical changes in the EEG signal. This phenomenon could not be detected by visual inspection of the original EEG signal or by other more traditional methods of signal processing. The nature of the phenomenon indicates that it may be possible to more accurately localize the

epileptogenic focus as well as to predict the onset of a seizure in time to intervene with abortive therapy.

Acknowledgment

This research is supported by a Research grant from the National Institute of Health (RO1 NS31451) and a Merit Review grant from the Department of Veterans Affairs, USA.

References

1. Iasemidis L.D., Zaveri H.P., Sackellares J.C. & Williams W.J., Linear and nonlinear modeling of ECoG in temporal lobe epilepsy, Proceedings of the 25th Annual Rocky Mountains Bioengineering Symposium, vol. 24, pp. 187-193, 1988.
2. Iasemidis L.D., Principe J.C. & Sackellares J.C., Spatiotemporal dynamics of human epileptic seizures, In: *3rd Experimental Chaos Conference*, Eds. R.G. Harrison, W. Lu, W. Ditto, L. Pecora, M. Spano & S. Vohra, World Scientific, Singapore, pp. 26-30, 1996.
3. Casdagli M., Iasemidis L.D., Sackellares J.C., Roper S.N., Gilmore R.L. & Savit R.S., Characterizing nonlinearity in invasive EEG recordings from temporal lobe epilepsy, *Physica D*, vol. 99, pp. 381-399, 1996.
4. Casdagli M., Iasemidis L.D., Gilmore R.L., Roper S.N., Savit R.S. & Sackellares J.C., Nonlinearity in invasive EEG recordings from patients with temporal lobe epilepsy, *Electroenceph. Clin. Neurophysiol.*, vol. 102, pp. 98-105, 1997.
5. Babloyantz A. & Destexhe A., Low dimensional chaos in an instance of epilepsy, *Proc. Natl. Acad. Sci. USA*, vol. 83, pp. 3513-3517, 1986.
6. Jansen B.H., Is it and so what? A critical review of EEG-chaos, In: *Measuring chaos in the human brain*, Eds. D. W. Duke & W.S. Pritchard, World Scientific, Singapore, pp. 83-96, 1991.
7. Elbert T., Ray W.J., Kowalik J., Skinner J.E., Graf K.E. & Birbaumer N., Chaos and physiology: deterministic chaos in excitable cell assemblies, *Physiol. Rev*., vol. 74, pp.1-47, 1994.
8. Freeman W.J., Strange attractors that govern mammalian brain dynamics shown by trajectories of electroencephalography (EEG) potentials, *IEEE Trans. Cas.* , vol. 35, pp. 781-784, 1988.
9. Kock C., Palovcik R. & Principe J.C., Chaotic activity during iron induced epileptiform discharges in rat hippocampal slices, *IEEE Trans. Biomed. Eng*., vol. 39, pp. 1152-1160, 1992.
10. Gevins A.S. & Remond A.R., *Handbook of electroencephalography and clinical neurophysiology*, Elsevier, Amsterdam, 1987.
11. Iasemidis L.D, *On the dynamics of the human brain in temporal lobe epilepsy*, Ph.D. Dissertation, University of Michigan, Ann Arbor, 1991.
12. Iasemidis L.D. & Sackellares J.C., The temporal evolution of the largest Lyapunov exponent on the human epileptic cortex, In: *Measuring chaos in the human brain*, Eds. D. W. Duke & W.S. Pritchard, World Scientific, Singapore, pp. 49-82, 1991.
13. Iasemidis L.D. & Sackellares J.C., Chaos theory in epilepsy, *The NeuroScientist*, vol. 2, pp. 118-126, 1996.
14. Holden A.V., *Chaos-nonlinear science: theory and applications*, Manchester University Press, Manchester, 1986.
15. Oppenheim A.V., Signal processing in the context of chaotic signals, *IEEE Int. Conf. ASSP*, vol. 4, pp. 117-120, 1992.
16. Lopes da Silva F., EEG analysis: theory and practice; Computer-assisted EEG diagnosis: pattern recognition techniques, In*: Electroencephalography; basic principles, clinical applications and related*

fields, Eds. E. Niedermeyer & F. Lopes da Silva F, Urban & Schwarzenburg, Baltimore, pp. 871-919, 1987.
17. Packard N.H., Crutchfield J.P., Farmer J.D. & Shaw R.S., Geometry from time series, *Phys. Rev. Lett*., vol. 45, pp. 712-716, 1980.
18. Takens F., Detecting strange attractors in turbulence, In:. *Dynamical systems and turbulence*, Lecture notes in mathematics, Eds. D.A. Rand & L.S. Young, Springer-Verlag, Heidelburg, pp. 366-381, 1981.
19. Grassberger P. & Procaccia I., Measuring the strangeness of strange attractors, *Physica D*, vol. 9, pp. 189-208, 1983.
20. Grassberger P., Schreiber T. & Schaffrath C., Nonlinear time sequence analysis, *Int. J. Bifurc. Chaos* vol. 1, pp. 521-547, 1991.
21. Mayer-Kress G, editor, *Dimension and entropies in chaotic systems*, Springer-Verlag, Berlin, 1986.
22. Kostelich E.J., Problems in estimating dynamics from data, *Physica D*, vol. 58, pp. 138-152, 1992.
23. Oseledec A., A multiplicative ergodic theorum—Lyapunov characteristic numbers for dynamical systems (English translation), *IEEE Int. Conf. ASSP*, vol. 19, pp. 179-210, 1968.
24. Pesin J., Characteristic Lyapunov exponents and smooth ergodic theory, *Russian Math. Survey*, vol. 4, pp. 55-114, 1977.
25. Walters P., *An introduction to ergodic theory*, Springer graduate text in mathematics, vol. 79, Springer-Verlag, Berlin, 1982.
26. Abarbanel H.D.I., *Analysis of observed chaotic data*, Springer-Verlag, New York, 1996.
27. Wolf A., Swift J.B., Swinney H.L. & Vastano J.A., Determining Lyapunov exponents from a time series, *Physica D*, vol. 16, pp. 285-317, 1985.
28. Iasemidis L.D., Sackellares J.C., Zaveri H.P. & Williams W.J., Phase space topography of the electrocorticogram and the Lyapunov exponent in partial seizures, *Brain Topogr*. vol. 2, pp. 187-201, 1990.
29. Eckmann J.P., Kamphorst S.O., Ruelle D. & Ciliberto S., Lyapunov exponents from times series. *Phys. Rev. A*, vol. 34, pp. 4971-4972, 1986.
30. Palus M., Albrecht V. & Dvorak I., Information theoretic test for nonlinearity in time series, *Phys. Lett. A*, vol. 175, pp. 203-209, 1993.
31. Vastano J.A. & Kostelich E.J., Comparison of algorithms for determining Lyapunov exponents from experimental data. In*: Dimensions and entropies in chaotic systems: quantification of complex behavior*, Ed. Mayer-Kress G., Springer-Verlag, Berlin, pp. 100-107,1986.
32. Frank W.G., Lookman T., Nerenberg M.A., Essex C., Lemieux J., & Blume W., Chaotic time series analyses of epileptic seizures, *Physica D*, vol. 46, pp. 427 – 438, 1990.
33. Wolf A., & Vastano J.A., Intermediate length scale effects in Lyapunov exponent estimation, In: *Dimensions and entropies in chaotic systems: quantification of complex behavior*, ed. G. Mayer – Kress, Springer-Verlag, Berlin, pp. 94 – 99, 1986.
34. Iasemidis L.D., Zaveri H.P., Sackellares J.C. & W.J. Williams, Phase space analysis of EEG, *IEEE EMBS*, 10th Annual Int. Conf., pp. 1201-1203, 1988.
35. Barlow J.S., Methods of analysis of nonstationary EEGs with emphasis on segmentation techniques: a comparative review, *J. Clin. Neurophysiology*, vol. 2, pp. 267–304, 1985.
36. Ferber G., Treatment of some nonstationarities in the EEG, *Neuropsychobiology*, vol. 17, pp. 100–104, 1987.
37. Jansen B.H. & Cheng W.K., Structural EEG analysis: an explorative study, *Int. J. Biomed. Comput.*, vol. 23, pp. 221–237, 1988.
38. Iasemidis L.D., Principe J.C., Czaplewski J.M., Gilmore, R.L., Roper S.N. & Sackellares J.C., Spatiotemporal transition to epileptic seizures: A non-linear dynamical analysis of scalp and intracranial EEG recordings, In: *Spatiotemporal Models in Biological and Artifical Systems*, Eds. F. Lopes da Silva, J.C. Principe & L.B. Almeida, IOS Press, Amsterdam, pp. 81-88, 1996.
39. Haken H., *Principles of brain functioning: a synergetic approach to brain activity, behaviour and cognition*, Springer series in Synergetics, vol. 67, Berlin, Springer-Verlag, Berlin, 1996.